Journal of Asian Earth Sciences 37 (2010) 246–258

Contents lists available at ScienceDirect

Journal of Asian Earth Sciences

journal homepage: www.elsevier.com/locate/jseaes

$^{40}Ar/^{39}Ar$ geochronology of post-collisional volcanism in the middle Gangdese Belt, southern Tibet

Su Zhou [a,*], Xuanxue Mo [a], Zhidan Zhao [a], Ruizhao Qiu [b], Yaoling Niu [c], Tieying Guo [a], Shuangquan Zhang [a]

[a] China University of Geoscience (Beijing), Beijing 100083, PR China
[b] Development and Research Center, China Geological Survey, Beijing 100037, PR China
[c] Department of Earth Sciences, Durham University, Durham DH1 3LE, UK

ARTICLE INFO

Article history:
Received 24 January 2008
Received in revised form 13 August 2009
Accepted 24 August 2009

Keywords:
$^{40}Ar/^{39}Ar$ geochronology
Post-collisional volcanism
Southern Tibet

ABSTRACT

^{40}Ar–^{39}Ar step-heating experiments on eleven mineral separates have been conducted on eight volcanic rocks and a granite-porphyry dike from the Yangying and Wuyu basins in the middle Gangdese Belt, southern Tibet. New radiometric ages for sanidine and biotite separates in four volcanic rock samples from Yangying ranges from 10.32 ± 0.07 to 11.40 ± 0.11 Ma, whereas plagioclase and biotite separates from a stratigraphic section of the Gaza Cun Formation in the Wuyu basin give ages from 12.57 ± 0.08 to 13.2 ± 0.2 Ma. A granite-porphyry which cuts the lower part of the Gaza Cun Formation gives an age of 11.09 ± 0.07 Ma, and a dacite from the margin of Wuyu basin gives an age of 15.48 ± 0.11 Ma. These age data, in conjunction with geochemical data, suggest that the mid-Miocene post-collisional volcanic rocks from these two basins have both similarities and difference in their petrogenesis. The high [Sm/Yb]*N* (>7) ratio and high Sr concentration (423–1065 ppm) in both suites are consistent with their parental melts derived from partial melting of eclogitized lower crust. However, the Yangying samples are more evolved than the Wuyu samples as manifested by lower MgO, Sr/Sr*, Eu/Eu*, and normative plagioclase. It is likely that the source material for the Yangying suite is likely more enriched in K_2O than that of the Wuyu suite, perhaps has a greater contribution from metasomatized lithospheric mantle. It is apparent that the post-collisional volcanism in southern Tibet occurred spatially scattered and temporally within a short period in each volcanic basin.

1. Introduction

The exact timing of the India–Asia continental collision remains debated, varying from ~70 to ~38 Ma (Beck et al., 1995; Searle, 1986; Searle et al., 1988; Klootwijk et al., 1992; Yin and Harrison, 2000; Mo et al., 2003, 2007; Zhou et al., 2004). Nevertheless, widespread tectonic and magmatic activities have continued on the Tibetan Plateau. High-K lavas have been erupting since ~13 Ma on the northern Tibetan Plateau. This is interpreted by some (Turner et al., 1993, 1996) as a consequence of thinning of the lithospheric mantle, marking the onset of the Tibetan plateau uplift. Others (e.g., Chung et al., 1998), however, argue that the uplift has been diachronous starting 40 Ma based on the observation that alkaline volcanism occurred from ~40 to 30 Ma in the eastern part of the plateau. Nevertheless, there are few geochronological data for post-collisional volcanic rocks for the southern region of the Tibetan plateau, because of their sparse distribution and limited volumes. The latter has thus hindered not only our understanding of the plateau-forming mechanism, but also our ability to quantify its process.

In this paper, we present in detail new $^{40}Ar/^{39}Ar$ age data on eleven mineral separates of nine rock samples from the middle Gangdese Belt in southern Tibet. These samples were taken from two volcanic fields, i.e., the Yangying and Wuyu basins, ~100 km apart from each other (Fig. 1). We interpret the age data along with geochemical data to discuss temporal and spatial distribution of post-collisional volcanism in the southern part of the Tibetan plateau and the petrogenesis.

2. Geological background and samples

One of our study locations, the Yangying geothermal field, is situated in Dangxiong County, Tibet along the China–Nepal road, about 80 km northwest of Lhasa and 55 km south of the well-known Yangbajing geothermal field (Fig. 1). It lies in one of the strings of graben basins trending generally northeast in the Gangdese Belt. The surrounding lithologies are mostly Mesozoic strata, including pre-Cretaceous slate and crystalline limestone to the northeast and Upper Cretaceous ignimbrites to the east and north-

* Corresponding author. Tel.: +86 01 82321028; fax: +86 01 82321983.
E-mail address: zhousu@cugb.edu.cn (S. Zhou).

1367-9120/$ - see front matter © 2009 Elsevier Ltd. All rights reserved.
doi:10.1016/j.jseaes.2009.08.011

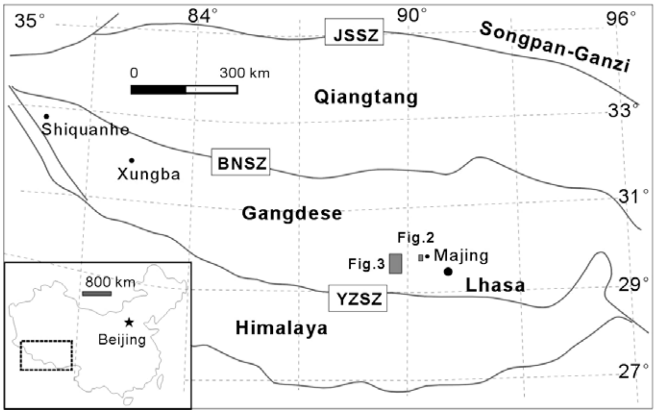

Fig. 1. Regional map of Tibet simplified from the 1:250,000 scale geologic map (Modified from Mo et al., 2008). Abbreviations: JSSZ, Jinshajiang Suture Zone; BNSZ, Bangong–Nujiang Suture Zone; YZSZ, Yarlung–Zangbo Suture Zone.

east. There are also Cenozoic strata consisting of Paleogene andesitic lavas and pyroclastic rocks to the north, Neogene dacitic pyroclastic rocks to the east and Pliocene trachyandesitic lavas and pyroclastic rocks to the west (Li et al., 1992). The strata within the geothermal field are mainly Cenozoic volcanic products, but dominated by Quaternary deposits with minor Paleogene rocks exposed at the center and northwestern part of the Yangying field (Fig. 2). The volcanic rocks of varying thickness are scattered over an area of about 10 km^2, and consist largely of pyroclastic deposits, subvolcanic intrusives as well as wildespread lava flows, extending north–south.

Pyroclastic rocks occur in the entrance of the Qialagai and Pujiemu valleys whereas subvolcanic rocks are mainly confined to the southernmost part of the geothermal field (Li et al., 1992). The stratigraphic relationship of pyroclastic rocks with subvolcanic rocks is yet to be confirmed. They both are previously attributed to the Linzizong succession (see 1/1,000,000 regional geological survey reports of Lhasa by XZBGMR, 1979). However, later studies using the whole-rock K–Ar method suggest that the volcanism at Yangying may be significantly younger and is geochemically much more alkalic (Li et al., 1992; Zhang, 1998). For this reason, we collected four samples along the Pujiemu valley and Qialagao valley in order to establish the relationship between these units and to improve the age data for the volcanism at the Yangying.

The other study location is in the Wuyu basin, Namling Country, about 200 km west of Lhasa, where the Wuyu Group crops out at its margin and is distributed in an ellipse area extending in NE–SW direction (Figs. 1 and 3). The Gaza Cun Formation is in the lower part of the Wuyu Group, which rests on andesitic rocks of the Dianzhong Formation (E_1d; basal unit of the Linzizong succession) with angular discordance and conformably underlies the Zongdang Cun Formation (N_2Z). The Gaza Cun Formation is subdivided into three parts: a lower trachytic section cut by granite-porphyry dikes, an upper pyroclastic section with caldera, and a middle section of coal-bearing clastic sedimentary rocks containing plant fossils and pollen grains of Pliocene age (1/200,000 Regional geological survey reports of Xietongmon and Namling (1996), Zhao et al. (2001); Fig. 4). No systematic geochronological study is avail-

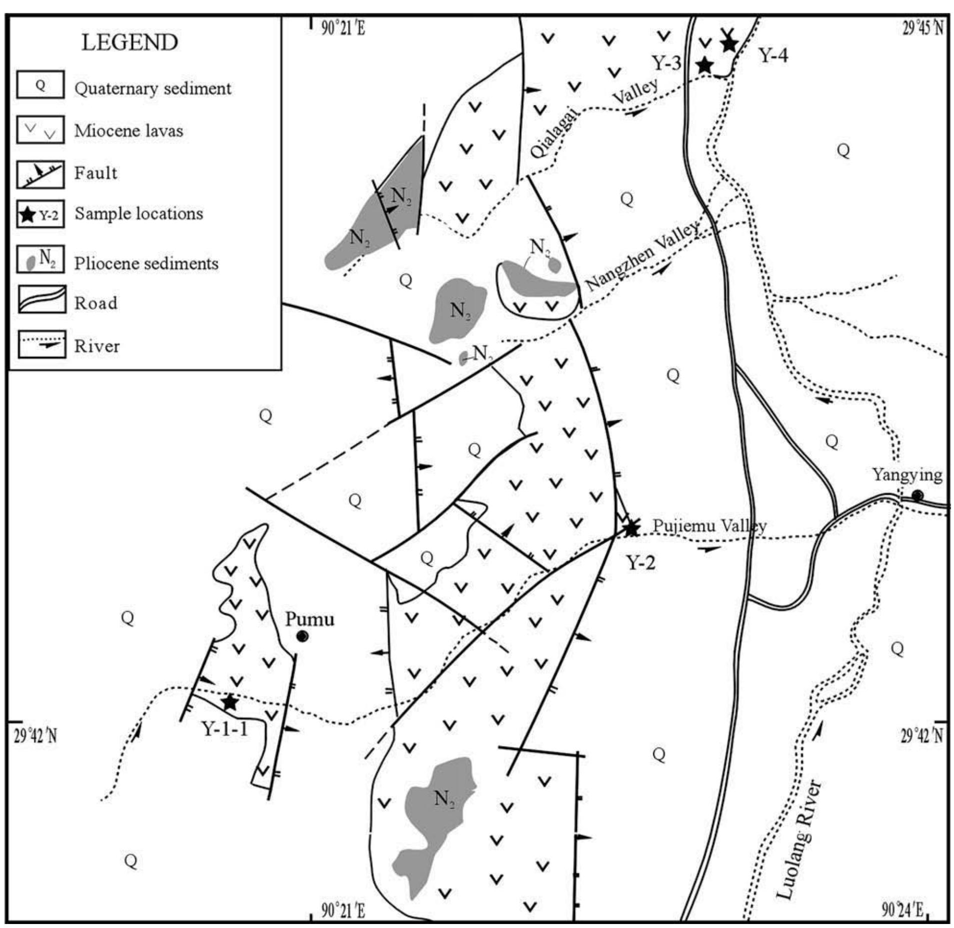

Fig. 2. Geological map showing distribution of the Cenozoic volcanic rocks in the Yangying geothermal field of Dangxiong district, Tibet, China (adapted from Li et al., 1992).

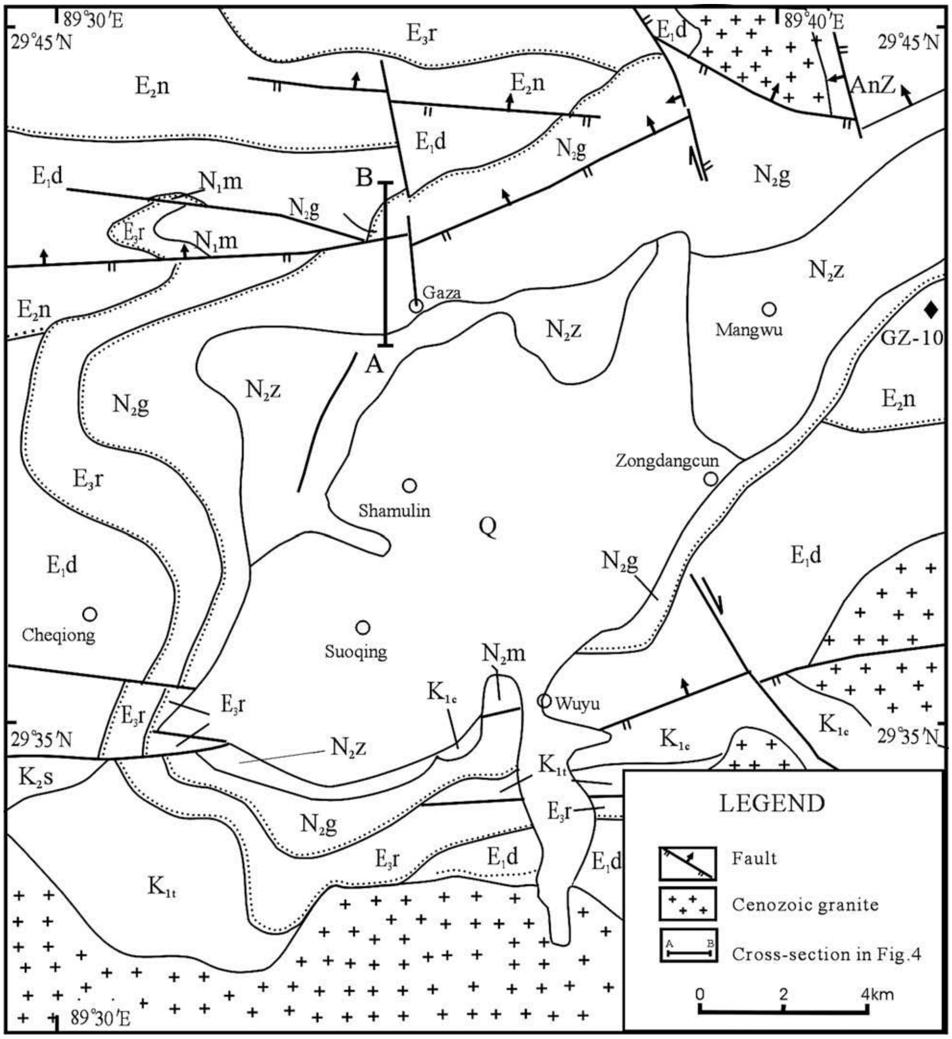

Fig. 3. Geological map of the Wuyu basin, Tibet (adapted from 1:200,000 map of XZBGMR (1996)). The symbols are: K_1c Chumulong and K_1t Takena Formation; E_1d, Dianzhong Formation; E_2n, Nianbo Formation; E_3r, Rigongla Formation; N_1m, Mangxiang Formation; N_2g, Gaza Cun Formation; N_2Z, Zongdancun Formation; Q, Quaternary.

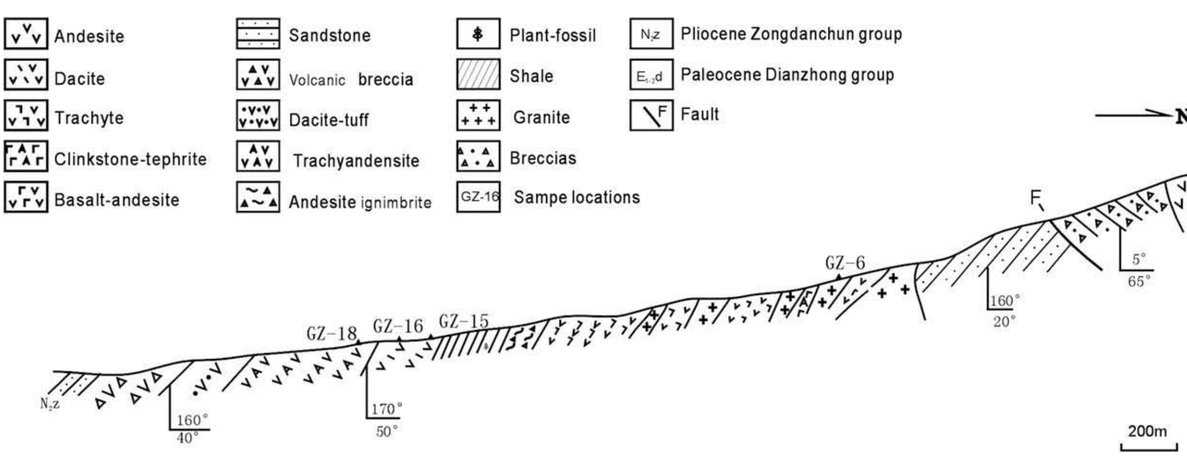

Fig. 4. Sketch of the cross-section studied (adapted from Zhang, 1998).

able for the Gaza Cun Formation although some dacitic lava flows/volcanogenic sediments were dated by ^{40}Ar–^{39}Ar to constrain the age of fossil leaf assemblages (Spicer et al., 2003). The ages of the Gaza Cun Formation were estimated based on stratigraphically equivalent dacite in Jiacuo to the northwest of the basin (18.5 ± 0.7 Ma) and volcanic rocks in the Coqen area about 300 km further to the northwest (10.3 Ma) using whole-rock K–Ar method (mentioned in the 1/200,000 Regional geological survey report of Xietongmon and Namling without giving actual data).

On the other hand, the recent 1/250,000 scale regional geological survey places the lower volcanic strata of the “Wuyu Group” in the Coqen area in the Dianzhong Formation (E_1d; basal unit of the

Linzizong succession) on the basis of (1) foraminiferal assemblageas (assigned to the Aptian to Cenomanian) and (2) 73.9 Ma K–Ar and 61.0 and 63.5 Ma Rb–Sr ages for dacite in the lower part of the "Wuyu Group" (Shi et al., 2001; Liu et al., 2004). These scattered age data require a further investigation.

Sample locations are shown in Figs. 2–4, respectively.

3. Brief petrography and major and trace element geochemistry

Trachyte samples Y-2 and Y-3 are porphyritic with a phenocryst assemblage of intermediate-acidic plagioclase, sanidine, biotite and clinopyroxene. Sanidine is fresh with resorption edges and well-developed twining. And plagioclase is partly altered, resulting in pseudomorphs and rimed by alkali-feldspar. Biotite with prominent opacity shows typically brown pleochroism. While trachyte GZ-16 is also porphyryitic with a phenocryst assemblage of Na-rich plagioclase, biotite and minor magnetite. The micrite matrix has the same mineralogy with trachytic texture.

High-K dacite GZ-10 and GZ-15 is porphyritic and has a phenocryst assemblage dominated by plagioclase of intermediate compositions with minor K-feldspar, biotite and quartz. Plagioclase is mostly twinned and zoned. Quartz is corroded. Groundmass has the same mineralogy.

GZ-18 (trachy-andesite) is porphyritic with a phenocryst assemblage of plagioclase, biotite, clinopyroxene and minor alkali-feldspar with magnetite. Plagioclase ranges from andesine to oligoclase in composition with fine euhedral oscillatory zoning, twining and slightly weak alteration. The groundmass has the same mineralogy.

The high-K rhyolite samples Y-1-1 and Y-4 contain a similar phenocryst assemblage to sample Y-2 (i.e., corroded quartz, fresh sanidine, and minor biotite with some obvious opacity) in a micrite to glassy groundmass. Granite-porphyry GZ-6 is porphyritic with a micrite matrix. K-feldspar and Na-rich plagioclase are common phenocrysts. The groundmass has the same mineralogy plus xenomorphic quartz. Some irregular carbonate veinlets are found in both phenocrysts and groundmass of the granite-porphyry.

Major element and trace element analyses (Table 1) were done by X-ray fluorescence spectrometer (XRF) and ICPMS respectively at the key laboratory of continental dynamics, Northwest University except sample GZ-16,18 which were analyzed at Tokyo Institute of Technology by X-ray fluorescence spectrometer (XRF).

Samples are alkali-rich (6.9% < $Na_2O + K_2O$ < 11.73%) with high Al_2O_3 (>14.21%, except for sample Y-4 which is 12.62%). The volcanic rocks are plotted in the field of Trachyte, dacite and rhyolite in TAS diagram (Fig. 5a, La Bas et al., 1986) except sample GZ-18 that is in the field of trachy-andesite on an anhydrous basis. Except Y-3, all samples belong to subalkaline varieties in TAS diagram (Irvine and Baragar, 1971). In K_2O versus SiO_2 plot, the samples vary significantly in K_2O and mostly plot in the fields of shoshonite (SHO) and high-potassium calc-alkaline (HK-CA) (Fig. 5b).

On chondrite-nonmalized rare-earth element (REE) diagram (Fig. 6), all of our samples display very similar patterns highly enriched in light REEs with a weak Eu anomaly ($Eu/Eu^* = 0.60–0.81$), suggesting the effect of plagioclase fractionation. Note that while the Linzizong volcanic rocks (e.g., samples D-15 for lower Dianzhong Formation, LZ994 for middle Nianbo Formation and P-1 for upper Pana Formation) are also enriched in light REEs, they differ from our samples from Wuyu and Yangying basins in having elevated abundances of heavy REEs (Fig. 6). On primitive mantle-normalized incompatible element diagrams, our samples show enrichments in Rb, Th, U and Pb with negative Sr, Nb, Ta, P and Ti anomalies (Fig. 7), which are apparently consistent with the influence of mature crustal materials.

Table 1
Major (wt.%) and trace element ($\times10^{-6}$) composition of the rocks from Wuyu and Yangying (Mo et al., in press)[a]

Sample No. Location	GZ-10 Wuyu	GZ-15 Wuyu	GZ-16 Wuyu	GZ-18 Wuyu	Y-1-1 Yangying	Y-3 Yangyong
SiO_2	64.07	66.31	64.75	61.34	68.60	68.22
TiO_2	0.52	0.53	0.64	0.59	0.69	0.47
Al_2O_3	15.80	15.72	16.54	15.18	14.07	15.24
TFe_2O_3	3.28	3.14	3.42	3.7	3.89	2.46
FeO	1.42	0.98	3.07	3.32	0.25	0.15
MnO	0.04	0.04	0.05	0.1	0.02	0.02
MgO	1.64	0.66	1.17	2.03	0.75	0.45
CaO	3.49	2.89	4.03	5.68	1.80	0.66
Na_2O	3.98	3.17	4.37	4.12	3.35	2.60
K_2O	3.16	3.73	3.06	2.9	5.20	9.13
P_2O_5	0.19	0.20	0.25	0.23	0.58	0.28
LOI	4.39	4.01			1.45	0.83
Total	100.56	100.40	97.95	95.49	100.40	100.36
K_2O/Na_2O	0.79	1.18	0.70	0.70	1.55	3.51
Li	26.8	52.4			3.4	84.6
Be	2.50	2.53			3.81	5.84
Sc	4.84	4.32			6.43	4.65
V	61.5	63.7			64.9	26.1
Cr	21.1	19.1			56.1	16.6
Co	3.0	0.9			1.7	<0.03
Ni	12.5	11.3	18.48	14.64	22.7	8.0
Cu	23.3	15.2			17.9	18.6
Zn	52.9	50.8			34.5	47.5
Ga	19.4	19.9			18.8	18.1
Ge	1.08	1.19			1.39	2.12
Rb	116	153	116.39	97.85	212	423
Sr	779	696	1030.4	965.51	1065	424
Zr	144	143	157.68	138.5	364	317
Nb	6.4	6.5	5.04	4.65	19.3	20.4
Cs	8.6	26.8			63.1	87.2
Ba	904	988	914.93	809.79	2359	1841
Hf	3.93	3.98			10.08	9.08
Ta	0.43	0.45			0.96	1.23
Pb	37.9	35.6	39	37.7	56.9	72.5
Th	18.7	19.5	19.96	16.77	55.1	64.4
U	3.7	3.3			7.3	11.5
La	26.7	27.2			82.1	76.3
Ce	55	56			169	149
Pr	6.8	6.8			24.0	20.1
Nd	26.0	26.4			90.4	71.3
Sm	4.3	4.3			13.4	10.2
Eu	1.02	1.01			2.70	1.85
Gd	3.22	3.26			9.84	8.20
Tb	0.35	0.35			0.96	0.83
Dy	1.64	1.62			4.09	3.71
Ho	0.26	0.25			0.55	0.57
Er	0.68	0.65			1.55	1.61
Tm	0.088	0.084			0.18	0.21
Yb	0.59	0.56			1.23	1.44
Lu	0.086	0.082			0.18	0.22
Y	7.7	7.6	7.08	6.95	18.1	17.5
$[La/Sm]_N$	4.01	4.08			3.96	4.83
$[Sm/Yb]_N$	8.10	8.52			12.11	7.87
Sr/Sr^*	1.684	1.495			0.657	0.320
Eu/Eu^*	0.804	0.792		0.687	0.599	
Ab + An	49.59	39.85	53.45	49.22	33.49	23.45
An/Ab	0.472	0.486	0.446	0.412	0.181	0.066

[a] See text for analytical details.

4. Ar–Ar geochronoloty

4.1. Analytical techniques

Samples for Ar–Ar dating were petrographically examined with care. Fresh and suitable samples (i.e., excluding those with obvious alteration and too fine-grained) were crushed, and separated

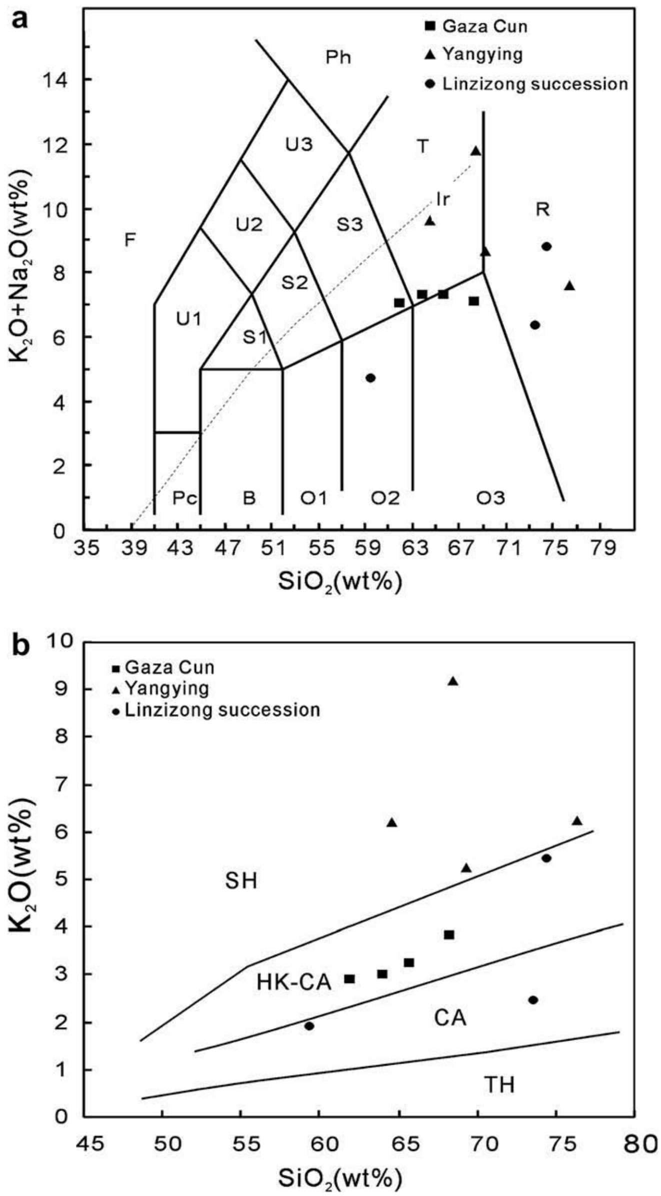

Fig. 5. Major element compositions of samples of this study plus representative samples from the synllisional Linzizong Volcanic Succession from the Linzhou Basin in (a) $K_2O + Na_2O$ vs. SiO_2 (after La Bas et al., 1986) and (b) K_2O vs. SiO_2 (Rickwood, 1989) spaces. Data for Y-2, Y-4 are from the literature (Nomade et al., 2004), and the others are new data of our research team (Table 1; Mo et al., in press). Symbols in (a) are: Pc, picrobasalt; B, basalt; O1, basaltic andesite; O2, andesite; O3, dacite; R, rhyolite; S1, trachybasalt; S2, basaltic trachy-andesite; S3, trachy-andesite; T, trachyte; U1, tephrite/basanite; U2, phono-tephrite; U3, tephri-phonolite; Ph, phonolite; F, foidite. Abbreviations in (b) are: SH, shoshonitic; HK-CA, high potassic calc-alkaline; CA, calc-alkaline; TH, tholeiitic. Linzizong succession of upper Pana, middle Nianbo and lower Dianzhong are shown for comparison (Mo et al., 2008).

using a combined method of heavy liquid and magnetic sorting for sanidine, biotite and plagioclase. These minerals were further picked for purity (>98%) under a microscope. The pure minerals were then cleaned in distilled water and acetone (in sequence) in an ultrasound bath to remove any surface contamination. The procedure was repeated several times until the solution was clear. The clean mineral separates were baked in an oven for 6 h at ~100 °C, weighed and wrapped in aluminum foil and placed along with the flux monitor ZBH-25 for each sample in a glass tube. The tube with a Cd jacket was irradiated in a rotating container for 8 h in the fast neutron nuclear reactor at Institute of Nuclear Energy of China in Beijing and received 4×10^{17} fast neutrons per cm^2. The ratio of thermal/fast neutrons is ca. 26.5/6.5. Subsequently, incremental step-heating analyses were done on a Micromass 5400 static vacuum mass spectrometer at the Geochronology Laboratory of China University of Geosciences (Beijing). The resistance-heated furnace used to extract argon from irradiated samples is monitored with an optical fiber thermocouple and controlled by feedback circuitry. In an increment-heating experiment the samples were pre-degassed at 300 °C for ~60 min and then heated to a given temperature for ten minutes while a Ti-sponge kept at 800 °C to purify the released gas. Eight to ten heating-increments were applied for each sample and the number of steps depended on the potassium content of the samples. After following purification on both Ti-sponge from 800 to 400 °C and Sorb–AC getter, the argon isotope composition of the samples were measured in a peak-hopping mode at the trap current of 200 μA and accelerating voltage of 4.5 KV. All valves were closed to maintain the system to static state during the process. Variations in mass spectrometer discrimination were corrected by analyzing splits of atmospheric Ar from a reservoir attached to the extraction system. Correction factors for isobaric interferences from K and Ca were used according to the experimental value for each step from the $^{39}Ar/^{37}Ar$ ratios. The fluence monitor, ZBH-25, was an interlaboratory standard biotite, which has an age of 133.2 Ma and is typically used in Chinese argon-dating laboratories, calibrated by international standards (Standard analyses methods for isotopic samples, 1997).

Isotope peak heights and errors were calculated by least-squares linear regression of eleven cycles to the time at which the mass spectrometer was equilibrated with the inlet section. An apparent age is calculated for the gas extracted at each heating-step after corrections are made for interfering Ar isotopes produced in the reactor. In calculating an apparent age it is assumed that the non-radiogenic Ar in a sample is atmospheric in isotopic composition, with a $^{40}Ar/^{36}Ar$ ratio of 295.5 (Nier, 1950).

Age spectra are calculated and displayed using the ISOPLOT software (version 2.31) designed by K. Ludwig at Berkeley Geochronology Center, USA (Ludwig, 1993). Isotope correlation (isochron) diagrams for both in $^{40}Ar/^{36}Ar$ versus $^{39}Ar/^{36}Ar$ and $^{39}Ar/^{40}Ar$ versus $^{36}Ar/^{40}Ar$ isotope correlation are drawn through the results for plateau gas fraction. For an age spectrum diagram, apparent ages are on the ordinate and incremental cumulative percentage of ^{39}Ar released on the abscissa. For the isochron diagram, $^{40}Ar/^{36}Ar$ is plotted on the ordinate and $^{39}Ar/^{36}Ar$ on the abscissa (Fig. 8). The slope of the isochron is $^{40}Ar_r/^{39}Ar_K$ (where subscript *r* indicates radiogenic and subscript K indicates K-derived), from which the age is calculated (Table 2). The errors assigned to the apparent age of an individual step, both $^{40}Ar/^{39}Ar$ plateau ages and, isochron ages, are 1σ uncertainties. These plateau and isochron ages are statistically indistinguishable. The intercepts of the isochron have $^{40}Ar/^{39}Ar$ ages that are not significantly different from 295.5. However, the precision of $^{40}Ar/^{39}Ar$ plateau age is generally better than the precision of isochron ages for the same sample due to the limited number of data points and/or difficulty in extrapolation of the intercept value from the narrow range of the data. Therefore, we chose the plateau age to represent the age of the dated igneous rock and give an example of the use of an isochron age and its plateau age for sanidines from sample Y-3 (Fig. 8d).

4.2. Results of $^{40}Ar/^{39}Ar$ analyses and synthesis

The apparent age spectrums for all samples are given in Figs. 8 and 9, respectively. An Appendix giving analytical data and isotope correlation diagrams, are available from the author upon request.

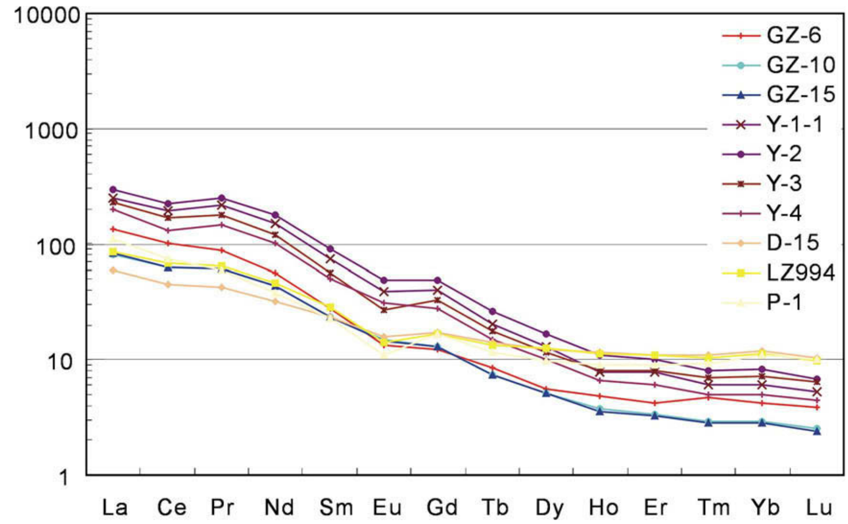

Fig. 6. Chondrite-normalized (Sun and McDonough, 1989) rare-earth element plots for samples. Data for Y-2, Y-4 and GZ-6 are from the literature (Nomade et al., 2004; Zhao et al., 2001), and the others are new data of our research team (Table 1; Mo et al., in press). Linzizong succession (rhyolitic upper Pana P-1, dacitic middle Nianbo LZ994 and andesitic lower Dianzhong D-15) (Mo et al., 2008) are shown for comparison.

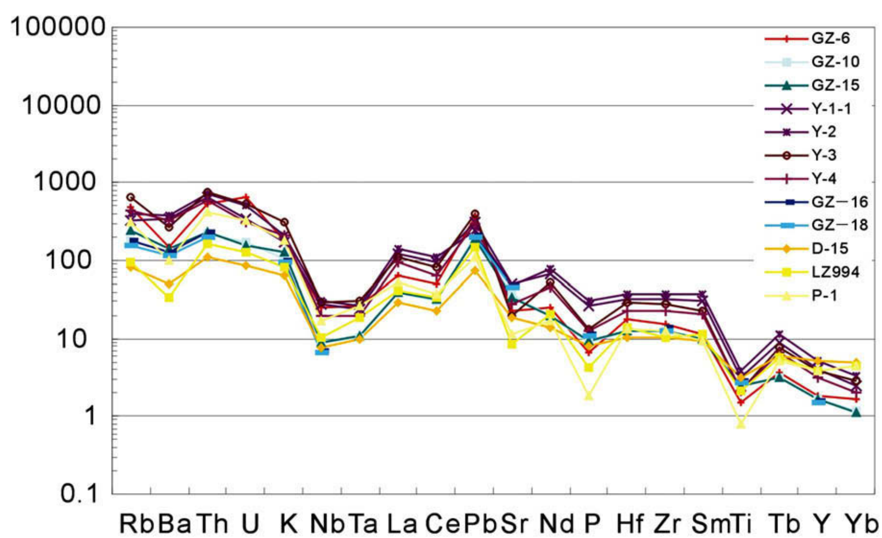

Fig. 7. Primitive mantle normalized (Sun and McDonough, 1989) trace element abundances for samples of this study. Data for Y-2, Y-4 and GZ-6 are from the literature (Nomade et al., 2004; Zhao et al., 2001), and the others are new data of our research team (Table 1; Mo et al., in press). Linzizong succession (rhyolitic upper Pana P-1, dacitic middle Nianbo LZ994 and andesitic lower Dianzhong D-15) (Mo et al., 2008) are shown for comparison.

4.2.1. Volcanic rocks from Yangying

Four sanidine and one biotite separate from four volcanic samples collected at Yangying yield similar $^{40}Ar/^{39}Ar$ released age spectra (Fig. 8a–f). Their spectra are characterized by initially slightly diverse apparent ages; this is likely caused by alteration products or some variation in the lattice defect of the minerals. Subsequent gases released define a broad plateau, encompassing about 77.4% of the total ^{39}Ar release for Y-1-1 (Fig. 8a), 80.1% for Y-2 (Fig. 8b), 79.2% for Y-3 (Fig. 8c) and 77.5% for subvolcanic rock Y-4 biotite (Fig. 8e), and 77.5% for Y-4 sanidine (Fig. 8f), with a plateau age of 11.40 ± 0.11, 10.73 ± 0.09, 11.14 ± 0.09, 10.32 ± 0.07 and 10.84 ± 0.08 Ma, respectively. The very slight ‘‘discrepancy’’ of the plateau age between sanidine and biotite in sample Y-4 may be related to the less argon retentivity of biotite compared with sanidine (McDougall and Harrison, 1999).

These results indicate that the Neogene volcanism at Yangying took place at 10.73 ± 0.09 to 11.40 ± 0.11 Ma with the subvolcanic rock being coeval (i.e., 10.84 ± 0.08 to 10.32 ± 0.07 Ma). These age data overlap earlier K–Ar determinations based on whole-rock samples (9.05–11.53 Ma; Li et al., 1992), and the volcanism was of short duration.

4.2.2. Volcanic rocks from the Wuyu basin

The age spectra of three plagioclase separates (GZ-15, GZ-16 and GZ-18) from volcanic rocks of Gaza Cun Formation at a stratigraphic section do not yield good plateaus(Fig. 9a, c and e), but give useful and significant results. Sample GZ-15 (plagioclase) from the lower site of the sampling traverse (Fig. 4) yields a saddle-shaped spectrum, which is interpreted to be related to excess argon as is typically shown in plagioclase. According to previous research on the pattern, the apparent age of the lowest portion in the spectrum could be taken as an upper limit to the cooling age of the mineral separates (Lanphere and Dalrymple, 1976). Thus, a weighed mean age of 13.2 ± 0.2 Ma of three contiguous bottom steps over 36.40% ^{39}Ar released (Fig. 9a) is interpreted as the age of plagioclase crystallization. Furthermore, biotite from the same sample provides a

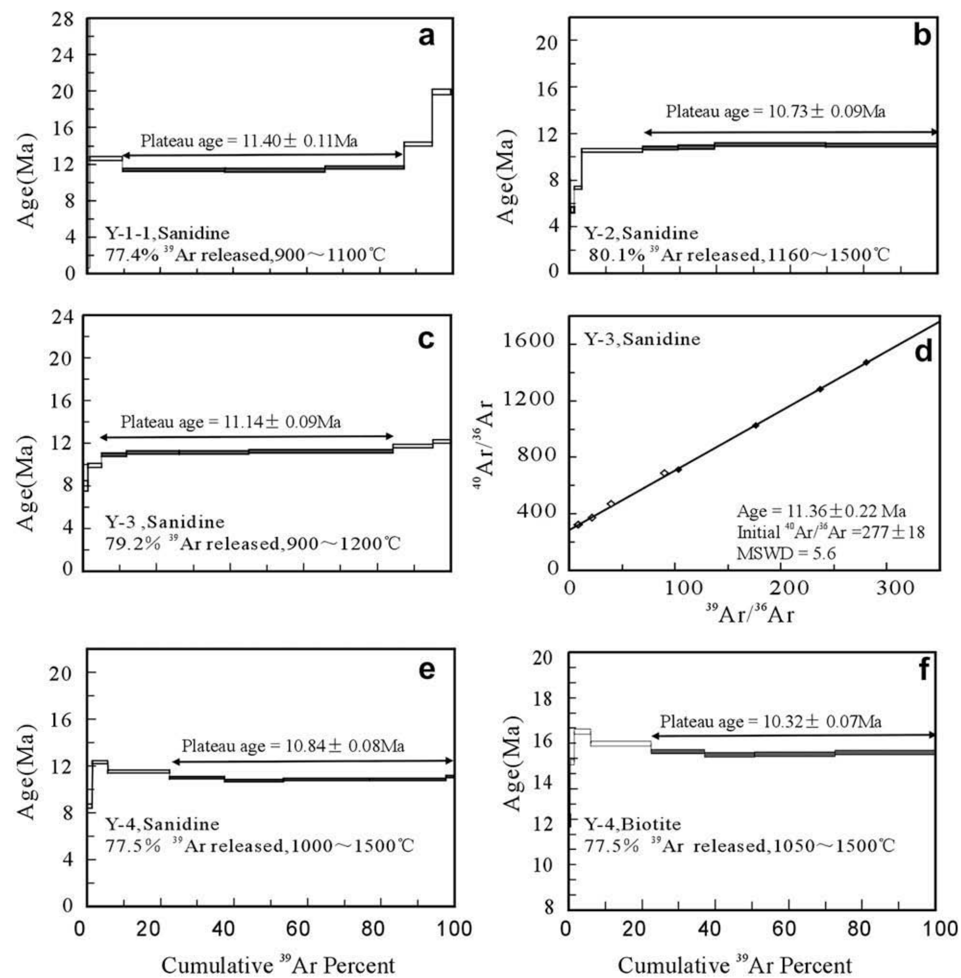

Fig. 8. $^{40}Ar/^{39}Ar$ age spectra and an isochron plot of volcanic rocks from Yangying, in the Gangdese Belt in southern Tibet.

Table 2
Age data for the Ganza Formation and Yangying volcanic rocks.

Sample No.	Rock name	Mineral	Total fusion age (Ma)	Plateau ^{39}Ar[a] (% (steps))	Plateau age (Ma)	Isochron age (Ma)	Isochron intercept
Y-1-1	High-K rhyolite	Sanidine	12.48	77.4(4–6)	11.40 ± 0.11	10.95 ± 0.32	363 ± 18
Y-2	Trachyte	Sanidine	10.87	80(7–10)	10.73 ± 0.09	11.5 ± 2.2	217 ± 220[b]
Y-3	Trachyte	Sanidine	11.18	79.2(4–7)	11.14 ± 0.09	11.38 ± 0.22	277 ± 18
Y-4	High-K rhyolite	Biotite	10.47	77.5(5–9)	10.32 ± 0.07	10.1 ± 1.9	326 ± 350[b]
Y-4	High-K rhyolite	Sanidine	10.99	77.5(6–9)	10.84 ± 0.08	10.78 ± 0.35	300 ± 41
GZ-10	High-K dacite	Plagioclase	16.76	43.8(4–7)	15.48 ± 0.11	14 ± 3	306 ± 18
GZ-15	High-K dacite	Plagioclase	13.09	36.4(4–6)			
GZ-15	High-K dacite	Biotite	13.13	84.6(5–8)	12.96 ± 0.07	13.28 ± 0.45	237 ± 91
GZ-16	Trachyte	Plagioclase	21.26	18.40(6)	13.63 ± 0.14[c]		
GZ-18	Trachy-andesite	Plagioclase	14.14	49.2(4–6)	12.57 ± 0.08	12.00 ± 0.13	311 ± 3
GZ-6	Granite granite	K-feldspar	11.36	87.28(5–8)	11.09 ± 0.07	10.86 ± 0.34	309 ± 29

Note: The values, for example, 11.09 ± 0.07 refers to mean ± 1σ.
[a] Percentage is proportion of the total ^{39}Ar defining the plateau. Steps are number of gas increments on the plateau.
[b] The abnormally high error of Isochron intercept is due to limited data and difficulty in extrapolation of the intercept value from the narrow range of the data.
[c] Concordant date for the bottom of steps.

plateau age of 12.96 ± 0.07 Ma between 9.6 and 94.2 cumulative% ^{39}Ar (a total of 84.6%) released (Fig. 9b), which is consistent with the age from plagioclase separate. Therefore, it is appropriate to neglect the excess argon fraction in plagioclase.

Two spectra of gas release on plagioclase for samples GZ-16 and GZ-18 from the middle and upper sites of the traverse bear considerable similarity. We interpret the depressed portion of the plagioclase spectrum of GZ-16 that gives 13.63 ± 0.14 Ma (including 18.4% of the total ^{39}Ar released, Fig. 9c) and the bottom three continuous steps of GZ-18 plagioclase that give 12.57 ± 0.08 Ma (including 49.2% of the ^{39}Ar release) as reflecting the timing of the volcanism (Fig. 9d), These give a maximum age for the two strata. Considering the stratigraphic positions along the traverse, it appears that sample GZ-16 may contain small amounts of excess Ar since the age for sample GZ-15 (13.2 Ma) should be older than the one for GZ-16 (13.63 Ma), while the age of sample GZ-18 (12.57 Ma) is reasonable.

A K-feldspar separate from the granite-porphyry dike (GZ-6) that cuts the traverse of the Gaza Cun Formation shows a broad plateau with a weighted mean age of 11.09 ± 0.07 Ma (with 12.8

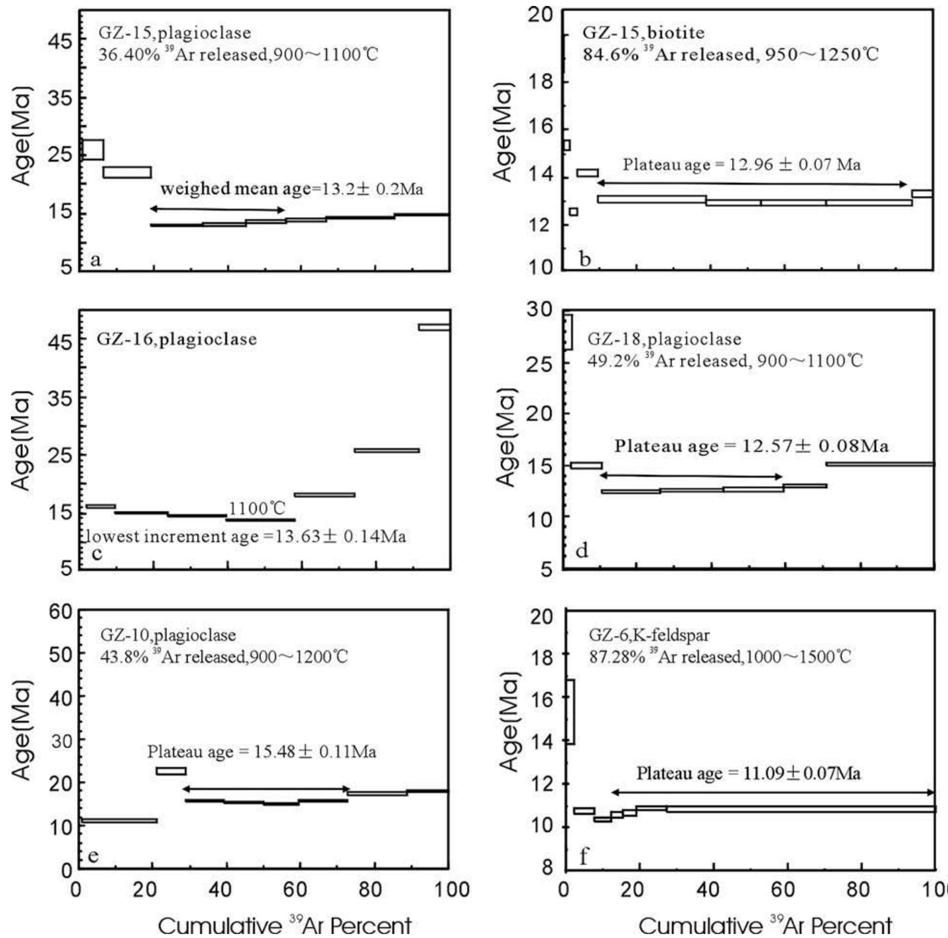

Fig. 9. $^{40}Ar/^{39}Ar$ age spectra of igneous rocks from the Wuyu basin in the Gangdese Belt in southern Tibet.

and 100% ^{39}Ar released; Fig. 9f), pacing a good constraint on the stratum age.

Plagioclase separates from dacite GZ-10, which is at the southeast margin of the basin, about 23 km to the Dazi–Namling road junction, also yields a disturbed age spectrum with a weighted mean $^{40}Ar/^{39}Ar$ plateau date of 15.48 ± 0.11 Ma (including 43.8% of the ^{39}Ar release), which is equivalent to the ages of dacitic lava flows and volcanogenic sediments (15.10 ± 0.49 to 14.03 ± 0.37 Ma, Spicer et al., 2003), giving the age of the lower stratigraphic level of the Gaza Cun Formation (Fig. 9e).

We can thus conclude that the volcanic eruption at the Wuyu basin took place from 15.48 ± 0.11 to 12.57 ± 0.08 Ma, and over a period of covered ~3 Myrs with younger dikes.

The $^{40}Ar/^{39}Ar$ data are summarized in Table 2, which gives plateau ages from age spectrum diagrams, the number of gas increments forming the plateaus and the percentage of ^{39}Ar released.

5. Discussion and conclusion

1. Inter-laboratory check: In order to evaluate the data quality of our laboratory, aliquots of sample Y-2 and Y-4 were dated at Berkeley Geochronology Center, USA, using the Fish Canyon sanidine as fluence monitor conducted in a MAP 215 spectrometer with a multiplier as collector. The results of Berkeley Geochronology Center are Y-2: 10.67 ± 0.19 Ma (sanidine single grain), Y-4: 10.56 ± 0.15 Ma (sanidine 10 mg) and 10.85 ± 0.2 Ma (20 biotite grains, Nomade et al., 2004). The relative error of plateau ages for the data from between the two laboratories is from 0.7% to 5.6%, which is within the accepted analytical range considering the likely differences in experimental conditions and protocols (machine discrimination, loading cycles and bakeout, blank levels, heating schedule, irradiation conditions, etc.). In addition, we collected volcanic rocks at Majiang where Coulon et al. (1986) reported their data. The plateau age of plagioclase measured from these rocks using our laboratory procedure is 10.80 ± 0.05 Ma (44.4% ^{39}Ar released), which agrees well with the results of T323, T324 (10.5 ± 0.4 and 10.1 ± 0.2 Ma; Coulon et al., 1986). These inter-lab checks attest that the data presented by our laboratory are reliable.
2. Our systematic Ar–Ar chronological studies reported here demonstrate that the Neogene volcanic activities at Yangying took place from 11.40 ± 0.11 to 10.32 ± 0.07 Ma, whereas those within Wuyu basin from 15.48 ± 0.11 to 12.57 ± 0.08 Ma. These are significantly younger than the syncollisional Linzizong succession (~ 65–40 Ma) temporarily associated with the India–Asia collision (Mo et al., 2003, 2007; Zhou et al., 2004; Yin and Harrison, 2000). The mid-Miocene volcanic rocks resemble the Linzizong succession in terms of Nd, Ta, P and Ti depletion, and enrichment of Pb, K and other large ion lithophile elements except for Sr that is slightly depleted (Fig. 7). However, their significant fractionation between light REEs and heavy REEs (e.g., $27 < [La/Yb]_N < 40$) (Fig. 6) and lower $\varepsilon_{Nd}[<-3.7]$ and

Table 3
Sr/Nd isotopic composition of the rocks from Wuyu, Yangying in southern Tibet (Mo et al., in press).

No.	Rb (ppm)	Sr (ppm)	$^{87}Rb/^{86}Sr$	$^{87}Sr/^{86}Sr$	2σ	Sm (ppm)	Nd (ppm)	Sm/Nd	$^{147}Sm/^{144}Nd$	$^{143}Nd/^{144}Nd$	2σ	ε_{Nd}
GZ-10	113.59	736.2	0.5160	0.706557	11	3.04	19.80	0.1536	0.0929	0.511641	5	−3.81
GZ-15	182.77	588.6	0.8988	0.706638	10	3.84	23.91	0.1605	0.0971	0.511646	6	−3.71
Y-1-1	241.68	1053.8	0.6638	0.712227	10	9.68	67.91	0.1425	0.0862	0.511427	6	−7.99
Y-2	230.26	714.4	0.9329	0.712179	9	9.49	66.12	0.1435	0.0868	0.511417	6	−8.19
Y-3	478.28	423.3	3.2702	0.710797	10	7.79	62.89	0.1238	0.0749	0.511513	6	−6.31
Y-4	139.79	369.8	1.0942	0.711226	11	6.62	45.22	0.1464	0.0885	0.511441	6	−7.72

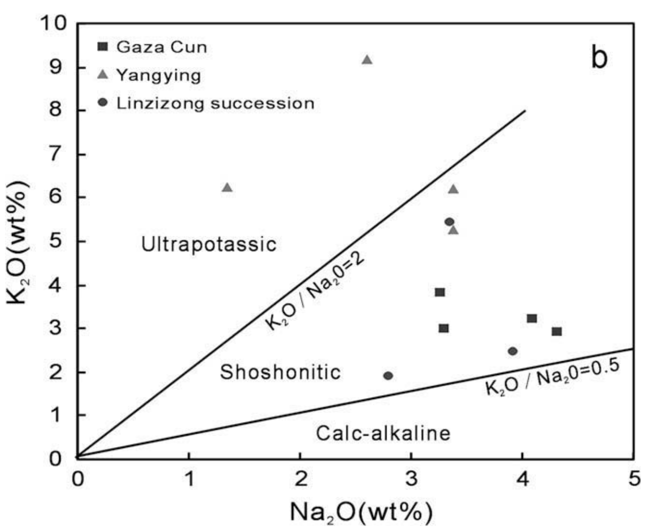

Fig. 10. K_2O vs. Na_2O plots. Data for Y-2 and Y-4 are from the literature (Nomade et al., 2004), and the others are new data of our research team (Table 1; Mo et al., in press). Linzizong succession of upper Pana, middle Nianbo and lower Dianzhong (Mo et al., 2008) are shown for comparison.

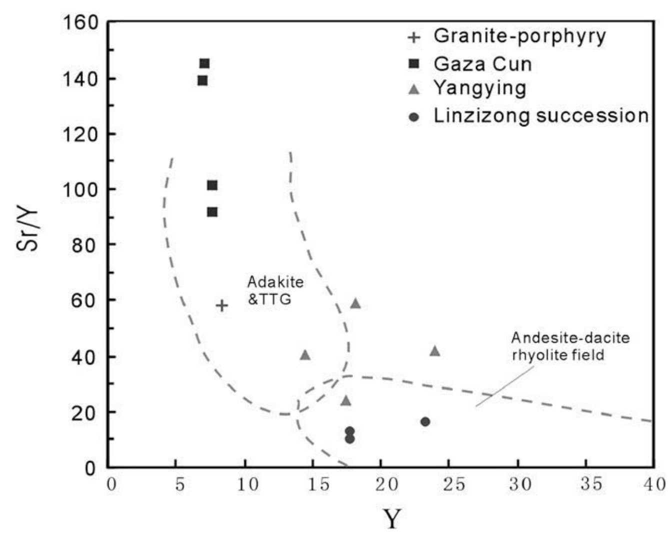

Fig. 11. Sr/Y vs. Y plots (Drummond and Defant, 1990), showing fields of adakites and arc intermediate-felsic rocks. Data for Y-2, Y-4 and granite-porphyry rock are from literature (Nomade et al., 2004; Zhao et al., 2001), and the others are new data of our research team (Table 1; Mo et al., in press). Linzizong succession of upper Pana, middle Nianbo and lower Dianzhong (Mo et al., 2008) are shown for comparison.

higher $[^{87}Sr/^{86}Sr]_i$ [<0.712227] differ significantly from the older Linzizong succession (e.g., $(6 < [La/Yb]_N < 12)$, $-4 < \varepsilon_{Nd} < +9.2$ and $0.704690 < [^{87}Sr/^{86}Sr]_I < 0.708316$) (Tables 1 and 3; Fig. 6; Zhou, 2002; Mo et al., 2008), showing their characteristic of post-collisional magmatism (Liegeois, 1998).

3. In the K_2O versus SiO_2 diagram, samples from Yangying are distinctly enriched and scatted in K_2O compared to those from Wuyu basin, which displays a positive correlation (Fig. 5b). In the K_2O versus.Na_2O diagrams, all the samples from Yangying have higher K_2O at a given Na_2O (e.g., $K_2O/Na_2O > 1.55$) than those from the Wuyu basin (e.g., $K_2O/Na_2O = 0.70–1.18$ (Fig. 10). Also, samples from Yangying display low MgO content (0.45–0.96%) and high Y content (14.5–24), whereas those from the Wuyu basin have higher MgO content (0.68–2.05%) and lower Y (6.95–7.7), resembling modern adakites from circum-Pacific subduction zones (Table 1; Fig. 11; Drummond and Defant, 1990) with the exception of high K_2O in the Wuyu samples.
4. Some previous studies have also documented the existence of post-collisional volcanism in southern Tibetan. Coulon et al. (1986) reported $^{40}Ar/^{39}Ar$ ages of 10.1–15.8 Ma for mineral separates from rhyodacitic lavas and three ignimbritic tuffs from Majiang, which is between our two study areas (Fig. 1). Arnaud et al. (1992) reported K–Ar ages of 16–20 Ma for intermediate to silica volcanic rocks from Shiquanhe in southwestern Tibet. Miller et al. (1999) also reported $^{40}Ar/^{39}Ar$ ages falling within the range of 18–25 Ma for ultrapotassic and potassic rocks and 16–17 Ma for calc-alkaline lavas and pyroclastic rocks in the Xungba–Gegar region from southwestern Tibet (Fig. 1). However, a genuine petrogenetic understanding of the origin and process of post-collisional volcanism remains out of reach (e.g., Deng, 1989,1991; Turner et al., 1993, 1996; Chung et al., 1998; Liu, 1999; Ding et al., 1999,2003; Zhao et al., 2001; Lai and Liu, 2001; Williams et al., 2001, 2004; Mo et al., 2006; Guo et al., 2007).
5. In general, ultrapotassic (UP) and shoshonitic (P) lavas have been interpreted as deriving from a low degree partial melting of a metasomatized lithospheric mantle (e.g., phlogopite bearing peridotite; Turner et al., 1993; Arnaud et al., 1992). The calc-alkaline varieties including ‘adakites’ have been interpreted as deriving from partial melting of eclogitized lower crust (Chung et al., 2003; Hacker et al., 2000), where the presence of garnet as a residual phase would hold Y and heavy REE, thus resulting in lower Y values and elevated Sr/Y ratios (i.e., the familiar concept of “garnet signature”) in erupted lavas. If we were to follow this interpretation, then we would come to the conclusion that the samples from Wuyu basin may be adakitc and derived from eclogitized lower crust whereas the Yangying are not. However, the genuine garnet signature is not the absolute abundances of HREEs or Y, but ratios of intermediate REE over heavy REEs, e.g., $[Sm/Yb]_N$. Table 1 shows that the garnet signature is essentially the same for samples from the two locations, and if anything, the Yangying samples would have even stronger garnet signature. For example, sample Y-1-1 from Yangying has an $[Sm/Yb]_N$ ratio of 12, that is significantly higher than that for samples from the Wuyu basin (8.10 and 8.52 in Table 1). The lower MgO, Sr/Sr^*, Eu/Eu^*, and normative plagioclase (in particular the An/Ab ratio) of the Yangying sam-

ples than those of Wuyu samples (Table 1) suggest that the Yangying samples are significantly more evolved than the Wuyu ones by plagioclase-dominated fractional crystallization. Because Eu is much less incompatible than Sm and Gd in plagioclase, which explains greater negative Eu anomalies of the Yangying samples than the Wuyu samples, Furthermore, Sr is compatible whereas Pr and Nd are very incompatible in plagioclase, which explains the significantly greater negative Sr (vs. Eu) anomalies of Yangying samples than the Wuyu samples (see Niu and O'Hara, 2009, for details). Because Y and other REEs are similarly incompatible in plagioclase. The overall abundances of Y and REEs are higher in Yangying samples than in the Wuyu samples (Fig. 6). Therefore, the overall very high $[Sm/Yb]_N$ ratios in both sample suites are consistent with their parental (or "primitive") melts derived from eclogitized lower crust. It is important to note, however, that the source material for the Yangying suite is likely more enriched in K_2O than that of the Wuyu suite, perhaps has a greater contribution from metasomatized lithospheric mantle.

6. It is apparent that post-collisional volcanism in southern Tibet is restricted to a relatively short period in the two basins.

Acknowledgments

This research is supported by the National Natural Science Foundation of China (40572048, 40672044, 49772107, and 49802005), the National Key Project for Basic Research on the Tibetan Plateau (2009CB421000), the Chinese 111 Project (No. B0701) and National Basic Research Program of China (973 Program: 2009CB421002). We thank Xiuquan Luo, Dunyi Liu and Daming Li for analytical assistance/advice and their comments on the study. Dr. Kirkham and Mr. Tootell are thanked for their reading through an earlier draft and providing comments for improvement. We also thank John Gamble and Igor M. Villa for their thorough reviews of and constructive comments on an early version of the manuscript.

Appendix

Wuyu basin

Steps	Temperature (°C)	$^{40}Ar/^{39}Ar$	$^{36}Ar/^{39}Ar$	$^{37}Ar/^{39}Ar$	^{39}Ar (mol) ($\times 10^{-12}$)	^{39}Ar Cum (%)	Apparent age ± 1σ (in Ma)
GZ-6, K-feldspar, weigh = 0.2 g, J = 0.000781							
1	500	394.1228	1.194400	0.06384	0.015	0.11	57 ± 10
2	700	38.5025	0.092785	0.05564	0.441	3.25	15.54 ± 0.25
3	800	21.4836	0.044231	0.14312	0.704	5.20	11.82 ± 0.18
4	900	11.8430	0.013598	0.01839	0.563	4.16	10.98 ± 0.16
5	1000	12.1240	0.014499	0.01351	0.619	4.57	11.00 ± 0.16
6	1100	13.6713	0.019238	0.01288	0.655	4.84	11.21 ± 0.16
7	1200	13.7825	0.019817	0.01162	1.116	8.24	11.12 ± 0.16
8	1500	13.4522	0.018649	0.00428	9.430	69.63	11.14 ± 0.16
Total age **=** 11.36 Ma							
GZ-10, plagioclase, weigh = 0.25g, J = 0.001273							
1	550	1059.1711	3.371057	0.25715	0.015	0.79	139 ± 53
2	700	59.7195	0.185681	0.19629	0.375	20.10	11.13 ± 0.41
3	800	91.1411	0.275225	1.22999	0.149	7.99	22.60 ± 0.64
4	900	32.2460	0.086517	2.08777	0.196	10.48	15.63 ± 0.23
5	1000	27.9994	0.072522	2.17666	0.200	10.71	15.39 ± 0.21
6	1100	24.4712	0.060874	1.86414	0.177	9.47	15.14 ± 0.22
7	1200	29.4637	0.076841	1.90546	0.245	13.11	15.77 ± 0.22
8	1300	38.8148	0.106147	2.37200	0.300	16.07	17.43 ± 0.22
9	1500	31.7955	0.081530	2.48521	0.210	11.28	18.03 ± 0.21
Total age **=** 16.76 Ma							
GZ-15, plagioclase, weigh = 0.23g, J = 0.001439							
1	550	508.5071	1.633065	1.08719	0.015	0.85	66 ± 16
2	700	120.9439	0.375838	2.45202	0.103	5.75	25.95 ± 1.74
3	800	107.7015	0.339801	16.02226	0.229	12.84	22.00 ± 0.84
4	900	16.9185	0.042092	7.28853	0.245	13.71	12.98 ± 0.16
5	1000	14.1083	0.031194	2.10999	0.215	12.00	13.04 ± 0.19
6	1100	16.9028	0.039805	1.59038	0.191	10.69	13.59 ± 0.20
7	1200	18.1291	0.043599	1.40901	0.190	10.64	13.82 ± 0.20
8	1300	19.7400	0.048539	1.79332	0.335	18.73	14.29 ± 0.18
9	1500	20.6344	0.050998	2.30722	0.265	14.80	14.82 ± 0.17
Total age **=** 13.09 Ma							
GZ-15, biotite, weigh = 0.21 g, J = 0.001428							
1	550	51.6262	0.149362	0.02452	0.091	0.59	19.18 ± 0.76
2	650	15.6426	0.032666	0.02839	0.232	1.50	15.36 ± 0.19
3	750	10.5480	0.019151	0.03356	0.288	1.86	12.54 ± 0.14
4	850	10.4240	0.016591	0.00942	0.874	5.65	14.16 ± 0.14
5	950	5.5158	0.001404	0.00168	4.506	29.15	13.08 ± 0.13

(continued on next page)

Appendix (*continued*)

Steps	Temperature (°C)	$^{40}Ar/^{39}Ar$	$^{36}Ar/^{39}Ar$	$^{37}Ar/^{39}Ar$	^{39}Ar (mol) ($\times 10^{-12}$)	^{39}Ar Cum (%)	Apparent age ± 1σ (in Ma)
6	1050	5.8367	0.002681	0.00117	2.277	14.73	12.94 ± 0.13
7	1150	5.7151	0.002288	0.00107	2.741	17.73	12.92 ± 0.13
8	1250	5.6383	0.002038	0.00100	3.555	23.00	12.92 ± 0.13
9	1500	7.4437	0.007645	0.01574	0.895	5.79	13.30 ± 0.13
Total age **=** 13.13 Ma							
GZ-16, plagioclase, weigh = 0.29 g, J = 0.001382							
1	550	966.2784	2.548101	0.93964	0.003	0.11	466 ± 283
2	700	69.9019	0.134259	1.69131	0.040	1.75	74.20 ± 1.03
3	800	29.4486	0.078260	1.72597	0.178	7.84	16.01 ± 0.23
4	900	10.3066	0.015180	1.87232	0.320	14.05	14.79 ± 0.16
5	1000	9.7318	0.013967	2.06263	0.359	15.80	14.29 ± 0.16
6	1100	8.9838	0.012329	2.00177	0.418	18.40	13.63 ± 0.14
7	1200	11.9070	0.016381	1.92466	0.368	16.17	17.88 ± 0.19
8	1300	15.5240	0.018063	2.25845	0.396	17.39	25.65 ± 0.26
9	1500	31.0321	0.041106	2.29971	0.193	8.48	46.95 ± 0.48
Total age **=** 21.26 Ma							
GZ-18, plagioclase, weigh = 0.29 g, J = 0.001314							
1	500	3934.8476	12.850890	15.91588	0.001	0.05	305 ± 3064
2	700	84.4018	0.245517	1.70529	0.041	2.03	28.19 ± 1.67
3	800	31.8826	0.086679	1.86454	0.167	8.33	15.12 ± 0.26
4	900	9.9473	0.016105	2.12943	0.314	15.69	12.62 ± 0.14
5	1000	10.1839	0.016816	2.23667	0.346	17.30	12.70 ± 0.13
6	1100	10.4967	0.017742	2.21659	0.324	16.20	12.79 ± 0.15
7	1200	13.4121	0.027092	2.16849	0.232	11.57	13.14 ± 0.17
8	1500	13.4409	0.024246	2.33839	0.577	28.83	15.22 ± 0.16
Total age **=** 14.14 Ma							

Yangying

Steps	Temperature (°C)	$^{40}Ar/^{39}Ar$	$^{36}Ar/^{39}Ar$	$^{37}Ar/^{39}Ar$	^{39}Ar (mol) ($\times 10^{-12}$)	^{39}Ar Cum (%)	Apparent age ± 1σ (in Ma)
*Y-1-1, sanidine, weigh = 0.4 g, **J** = 0.0008959*							
1	500	562.1494	1.748862	0.29114	0.015	0.39	71.9 ± 8.3
2	700	102.4945	0.287298	0.18473	0.023	0.59	28 ± 15
3	800	12.0909	0.014633	0.20705	0.345	8.72	12.53 ± 0.21
4	900	8.4489	0.004814	0.18610	1.121	28.36	11.34 ± 0.20
5	1000	8.2725	0.004381	0.28167	1.080	27.32	11.27 ± 0.21
6	1100	8.5938	0.004878	0.20973	0.857	21.69	11.54 ± 0.17
7	1200	11.3278	0.008436	0.13590	0.304	7.69	14.23 ± 0.20
8	1500	17.7592	0.017692	0.23893	0.208	5.26	20.16 ± 0.29
Total age = 12.48 Ma							
*Y-2, sanidine, weigh = 0.18 g, **J** = 0.0010863*							
1	550	697.3695	0.446393	0.16086	0.003	0.04	864 ± 61
2	700	299.0242	0.984860	0.05570	0.009	0.12	16 ± 12
3	800	87.2752	0.285139	0.01998	0.023	0.28	5.9 ± 2.2
4	900	27.3595	0.083188	0.01911	0.071	0.88	5.43 ± 0.25
5	1000	18.5286	0.050238	0.02069	0.160	1.97	7.20 ± 0.12
6	1100	7.2626	0.006703	0.03044	1.350	16.67	10.32 ± 0.14
7	1160	7.3838	0.006725	0.03123	0.764	9.42	10.54 ± 0.14
8	1220	7.1752	0.005913	0.03185	0.813	10.04	10.60 ± 0.15
9	1300	6.9510	0.004775	0.03247	2.457	30.32	10.82 ± 0.15
10	1500	7.3270	0.006118	0.03363	2.452	30.27	10.78 ± 0.15
Total age = 10.87 Ma							
*Y-3, sanidine, weigh = 0.12 g, **J** = 0.0014872*							
1	500	564.0207	1.863847	0.14244	0.001	0.07	35 ± 87
2	700	36.3202	0.112848	0.02001	0.105	1.23	7.95 ± 0.50
3	800	17.5211	0.046797	0.02367	0.321	3.76	9.87 ± 0.17
4	900	6.9477	0.009704	0.03099	0.575	6.72	10.91 ± 0.16
5	1000	5.8282	0.005682	0.03212	1.239	14.48	11.09 ± 0.16
6	1100	5.4122	0.004233	0.03201	1.613	18.85	11.12 ± 0.16
7	1200	5.2500	0.003577	0.03192	3.352	39.17	11.21 ± 0.16

Appendix (*continued*)

Steps	Temperature (°C)	$^{40}Ar/^{39}Ar$	$^{36}Ar/^{39}Ar$	$^{37}Ar/^{39}Ar$	^{39}Ar (mol) ($\times 10^{-12}$)	^{39}Ar Cum (%)	Apparent age ± 1σ (in Ma)
8	1300	7.6568	0.011119	0.03352	0.930	10.87	11.67 ± 0.18
9	1500	12.0052	0.025284	0.03572	0.415	4.85	12.12 ± 0.18
Total age = 11.18 Ma							
Y-4, sanidine, weigh = 0.22 g, ***J*** *= 0.0013000*							
1	500	133.8239	0.432875	0.01880	0.017	0.09	13.80 ± 8.8
2	700	20.8301	0.058146	0.01277	0.235	1.29	8.53 ± 0.20
3	800	12.9485	0.025965	0.00664	0.784	4.31	12.32 ± 0.18
4	900	5.5966	0.002268	0.00407	3.050	16.77	11.51 ± 0.16
5	1000	5.4921	0.002681	0.00591	2.721	14.96	10.98 ± 0.16
6	1100	5.4216	0.002788	0.00839	2.908	15.99	10.74 ± 0.15
7	1200	5.3850	0.002554	0.00884	4.280	23.53	10.82 ± 0.15
8	1300	5.2842	0.002193	0.01006	3.765	20.70	10.83 ± 0.15
9	1500	10.9180	0.020887	0.02129	0.428	2.35	11.09 ± 0.16
Total age = 10.99 Ma							
Y-4, biotite, weigh = 0.23 g, ***J*** *= 0.0012726*							
1	550	86.1232	0.276178	0.02043	0.030	0.16	10.3 ± 3.1
2	650	26.6170	0.081345	0.01714	0.086	0.47	5.90 ± 0.42
3	750	15.8389	0.039177	0.01048	0.170	0.93	9.75 ± 0.19
4	850	11.7046	0.022212	0.00698	0.818	4.47	11.75 ± 0.17
5	950	5.4515	0.002210	0.00425	3.011	16.43	10.97 ± 0.16
6	1050	5.2187	0.002221	0.00683	2.694	14.70	10.43 ± 0.15
7	1150	5.1736	0.002386	0.00917	2.488	13.57	10.22 ± 0.14
8	1250	5.0601	0.001946	0.00974	4.017	21.92	10.26 ± 0.15
9	1500	5.5640	0.003481	0.01292	5.013	27.35	10.37 ± 0.15
Total age = 10.47 Ma							

Argon isotopic results for analysed samples. Reported errors are 1 sigma (1σ) for plateau and total ages, which include uncertainties of the monitors and their $^{40}Ar/^{39}Ar$ ratios. Correction interference used for $^{36}Ar/^{37}Ar_{Ca}$ is 2.398×10^{-4}. Mass discrimination factor is calculated for $^{40}Ar/^{36}Ar$ ratio of 295.5.

References

Arnaud, N.O., Vidal, Ph., Tapponnier, P., Matter, Ph., Deng, W.M., 1992. The high K_2O volcanism of northwestern Tibet: geochemistry and tectonic implications. Earth and Planetary Science Letters 111, 351–367.

Beck, R.A., Burbank, D.W., Sercombe, W.J., et al., 1995. Stratigraphic evidence for an early collision between northwest India and Asia. Nature 373, 55–58.

Chung, S.L., Lo, C.H., Lee, T.Y., Zhang, Y., Xie, Y., Li, X., Wang, K.L., Wang, P.L., 1998. Diachronous uplift of the Tibetan plateau starting 40 Myr age. Nature 394, 769–773.

Chung, S.L., Ji, D.L.J., Chu, M.F., Lee, H.Y., Wen, D.J., Lo, C.H., Qian, T.Y.L.Q., Zhang, Q., 2003. Adakite from continental collision zones: melting of thickened lower crust beneath southern Tibet. Geology 31, 1021–1024.

Coulon, C., Maluski, H., Bollinger, C., et al., 1986. Mesozoic and Cenozoic volcanic rocks from central and southern Tibet ^{39}Ar–^{40}Ar dating, petrogical characteristics and geogynamical significance. Earth and Planetary Science Letter 79, 281–302.

Deng, W., 1989. Cenozoic volcanic rocks in the northern Ngari district of the Tibet: a discussion on the intracontinental subduction. Acta Petrologica Sinica 3, 1–11 (in Chinese with English abstract).

Deng, W., 1991. Geology, geochemistry and ages of the shoshonitic lavas in the central Kunlun orogenic belt. Scientia Geologica Sinica 3, 201–213 (in Chinese with English abstract).

Ding, L., Kapp, P., Zhong, D., Deng, W., 2003. Cenozoic volcanism in Tibet: evidence for a transition from oceanic to continental subduction. Journal of Petrology 44, 1833–1865.

Ding, L., Zhang, J., Zhou, Y., 1999. Tectonic implications on the lithosphere evolution of Tibet Plateau: petrology and geochemistry of sodic and ultrapotassic volcanism in Northern Tibet. Acta Petrologica Sinica 15 (3), 408–421 (in Chinese with English abstract).

Drummond, M.S., Defant, M.J., 1990. A model for trondhjemite-tonalit-dacite genesis and crustal growth via slab melting. Archean to modern comparisons. Journal of Geophyscial Research 95, 21503–21521.

Guo, Z., Wilson, M., Liu, J., 2007. Post-collisional adakites in south Tibet: products of partial melting of subduction-modified lower crust. Lithos 96 (1–2), 205–224.

Hacker, B.R., Gnos, E., Ratshbacher, L., Grove, M., McWilliams, M., Sobolev, S.V., Wan, J., Zhenhan, W., 2000. Hot and dry deep crustal xenolihs from Tibet. Science 287, 2463–2466.

Irvine, T.N., Baragar, W.R.A.A., 1971. Guide to the chemical classification to the common volcanic rocks. Canadian Journal of Earth Sciences 8, 523–548.

Klootwijk, C.T., Gee, F.S., Peirce, J.W., et al., 1992. An early India contact: paleomagnetic constraints from Ninetyeast Ridge, ODP Leg 121. Geology 20, 395–398.

La Bas, M.J., Le Maitre, R.W., Streckeisen, A., Zanettin, B., 1986. A chemical classification of volcanic rocks based on the total alkali–silica diagram. Journal of Petrology 27, 745–750.

Lai, S., Liu, C., 2001. Enriched upper mantle and eclogitic lower crust in north Qiangtang, Qinghai–Tibet plateau: petrological and geochemical evidences from the Cenozoic volcanic rocks. Acta Petrologica Sinica 17, 459–468 (in Chinese with English abstract).

Lanphere, M.A., Dalrymple, C.B., 1976. Identification of excess $^{40}Ar/^{39}Ar$ age spectrum technique. Earth and Planetary Science Letters 32, 141–148.

Li, J.Z., Zhang, Y.Y., Luo, H.Y., 1992. A research on petrological characters and genesis of the Cenozoic volcanic rocks in the Yangying village Geothermal field, Dangxiong, Tibet, China. Geoscience 6 (1), 96–109 (in Chinese with English abstract).

Liegeois, J.P., 1998. Preface-some words on the post-collisional magmatism. Lithos 45, XV–XVII.

Liu, D.Z., Ma, R.Z., Tao, X.F., Hu, X.W., Shi, H., Zhu, L.D., Hu, X.W., 2004. New results and major progress in regional geology survey of the Coqen County sheet. Geological bulletin of China 23 (5–6), 506–511 (in Chinese with English abstract).

Liu, J., 1999. Volcanoes in China. Science Press, Beijing (p. 219; in Chinese with English abstract).

Ludwig, K.R., 1993. Isoplot: a plotting and regression program for radiogenic-isotope data: version 2.70, US Geological Survey Open-File Report 91-445, 41.

McDougall, I., Harrison, T.M., 1999. Geochronology and thermochronology by the $^{40}Ar/^{39}Ar$ Method, second ed. Oxford University Press, New York. p. 23.

Miller, C., Schuster, R., Klotzli, U., Mair, V., Frank, W., Purtscheller, F., 1999. Postcollisional potassic and ultra-potassic magmatism in SW Tibet: geochemical, Sr–Nd–Pb–O isotopic constraints for mantle source characteristics and petrogenesis. Journal of Petrology 83, 5361–5375.

Mo, X., Zhao, Z., Deng, J., Dong, G., Zhou, S., Guo, T.Y., Zhang, S.Q., Wang, L.L, 2003. Response of volcanism to the India–Asia collision. Earth Science Frontiers, 10(3), 135–148; (China University of Geosciences, Beijing; Chinese with English abstract).

Mo, X., Zhao, Z., Deng, J., Flower, M., Yu, X., Luo, Z., Li, Y., Zhou, S., Dong, G., Zhu, D., Wang, L., 2006. Petrology and geochemistry of postcollisional volcanic rocks from the Tibetan plateau: implications for lithosphere heterogeneity and collision-induced asthenospheric mantle flow. In: Dilek, Y., Pavlides, S., (Eds.), Postcollisional tectonics and magmatism in the Mediterranean region and Asia: Geological Society of America Special Paper 409. pp. 507–530.

Mo, Xuanxue, Niu, Yaoling, Dong, Guochen, Zhao, Zhidan, Hou, Zengqian, Zhou, Su, Ke, Shan, 2008. Contribution of syncollisional felsic magmatism to continental crust growth: a case study of the Paleogene Linzizong Volcanic Succession in southern Tibet. Chemical Geology 250, 49–67.

Mo, X., Hou, Z., Niu, Y., Dong, G., Qu, X., Zhao, Z., Yang, Z., 2007. Mantle contributions to crustal thickening in south Tibet in response to the India–Asia collision. Lithos 96, 225–242.

Mo, X., Zhao, Z., Guo, T., Yu, X., Deng, J., (Eds.), in press. Mesozoic–Cenozoic Tectono–Magmatism in Tibetan Plateau. Geological publishing house, Beijing.

Nier, A.O., 1950. A redetermination of the relative abundance of the isotopes of Carbon, Nitrogen, Oxygen, Argon, and Potassium. Physical Review 77, 789–793.

Niu, Y.L., O'Hara, M.J., 2009. MORB mantle hosts the missing Eu (Sr, Nb, Ta and Ti) in the continental crust: new perspectives on crustal growth, crust-mantle differentiation and chemical structure of oceanic upper mantle. Lithos. Doi: 10.1016/j.lithos.2008.12.009.

Nomade, S., Renne, P.R., Mo, X.X., Zhao, Z.D., Zhou, S., 2004. Miocene potassic and ultrapostassic volcanism in the Lhasa block: spatial trends and geodynamic implications. Earth and Planetary Science Letter 221, 227–243.

Rickwood, P.C., 1989. Boundary lines within petrologic diagrams which use oxides of major and minor elements. Lithos 55, 121–137.

Searle, M.P., 1986. Structural evolution and sequence of thrusting in the High Himalaya, Tibetan–Tethys and Indus suture zones of Zanskar and Ladakh, western Himalaya. Journal of Structural Geology 8, 923–936.

Searle, M.P., Cooper, D.J.W., Rex, A.J., 1988. Collision tectonics of the Ladakh–Zanskar Himalaya. Philosophical Transactions of the Royal Society, London A326, 117–150.

Shi, H., Ma, R.Z., Tao, X.F., Hu, X.W., Liao, C.G., Liu, D.Z., 2001. Advances in stratigraphy and paleontology in Coqen, Xizang with discussions on the role of paleontology in the geological surveying radiometric ages. Sedimentary Geology and Tethyan Geology 21 (2), 78–83 (In Chinese with English abstract).

Spicer, R., Harris, R.B.W., Widdowson, M., et al., 2003. Constant elevation of southern Tibet over the past 15 million years. Nature 421, 622–624.

Standard analyses methods for isotopic samples (DZ/T 0184.8-1997), 1997. Standard Publishing House, Beijing. pp. 62–69 (in Chinese).

Sun, S.S., McDonough, W.F., 1989. Chemical and isotope systematics of oceanic basalts: implications for mantle composition and processes. In: Saunders, A.D. (Ed.), Magmatism in Ocean Basins, vol. 42. Geological Society Publication, pp. 313–345.

Turner, S., Arnaud, N., Liu, J., Rogers, N., Hawkesworth, C., Harris, N., Kelley, S., Calsteren, P.V., Deng, W.M., 1996. Post-collisional, shoshonitic volcanism on the Tibetan Plateau: implications for convective thinning of the lithosphere and the source of ocean island basalts. Journal of petrology 37, 45–71.

Turner, S., Hawksworth, C., Lin, J.Q., Ogers, N., Kelley, S., Calsteren, P.V., 1993. Timing of Tibetan uplift constrained by analysis volcanic rocks. Nature 364, 50–53.

Williams, H., Turner, S., Kelley, S., et al., 2001. Age and composition of dikes in Southern Tibet: new constraints on timing of east–west extension and its relationship to post-collisional volcanism. Geology 29 (4), 339–342.

Williams, H.M., Turner, S.P., Pearce, J.A., Kelley, S.P., Harris, N.B.W., 2004. Nature of the source regions for postcollisional, potassic magmatism in southern and northern Tibet from geochemical variations and inverse trace element modeling. Journal of Petrology 45, 555–607.

XZBGMR (Xizang Bureau of Geology and Mineral Resources), 1979. Regional geological survey reports of Lhasa (scale 1:1,000,000) (in Chinese with English abstract).

XZBGMR (Xizang Bureau of Geology and Mineral Resources), 1996. Regional geological survey reports of Xietongmen and Namling (scale 1: 200,000) (in Chinese with English abstract).

Yin, A., Harrison, T.M., 2000. Geologic evolution of the Himalayan–Tibetan orogen. Annual Review of Earth and Planetary Sciences 28, 211–280.

Zhang, S.Q., 1998. The Characterististics of the Cenozoic post-collisional magmatism of the middle Gangdese, Tibet and its tectonic implications. Postdoctoral research report at Peking University (in Chinese with English abstract).

Zhao, Z.D., Mo, X.X., Zhang, S.Q., et al., 2001. Post-collisional magmatism in Wuyu basin, central Tibetet: evidence for recycling of subducted Tethyan oceanic crust. Science in China (Scientia Sinca), Series D 44 (Suppl.), 27–34.

Zhou, S., 2002. Study on the geochronology of several key regions of Gangdese magmatic and Yarlung Zangpo ophiolite belts, Tibet. Ph.D. Dissertation, China University of Geosciences, Beijing (in Chinese with English abstract).

Zhou, S., Mo, X.X., Dong, G.C., Zhao, Z.D., Qiu, R.Z., Guo, T.Y., Wang, L.L., 2004. ^{40}Ar–^{39}Ar geochronology of Cenozoic Linzizong succession from Linzhou Basin, Tibet, China, and their geological implications. Chinese Science Bulletin 49 (18), 1970–1979.